DESY 13-092
LPN 13-032
SFB/CPP-13-36

May 2013

Differential distributions for top-quark hadro-production with a running mass

M. Dowling[a] and S. Moch[a,b]

[a] *Deutsches Elektronensynchrotron DESY*
Platanenallee 6, D–15738 Zeuthen, Germany

[b] *II. Institut für Theoretische Physik, Universität Hamburg*
Luruper Chaussee 149, D–22761 Hamburg, Germany

Abstract

We take a look at how the differential distributions for top-quark production are affected by changing to the running mass scheme. Specifically we consider the transverse momentum, rapidity and pair-invariant mass distributions at NLO for the top-quark mass in the $\overline{\rm MS}$ scheme. It is found that, similar to the total cross section, the perturbative expansion converges faster and the scale dependence improves using the mass in the $\overline{\rm MS}$ scheme as opposed to the on-shell scheme. We also update the analysis for the total cross section using the now available full NNLO contribution.

The measurement of top-quark pair production cross sections at hadron colliders has entered the era of precision physics with the analysis of data available from the Large Hadron Collider (LHC) in the runs at center-of-mass energies $\sqrt{S} = 7$ and 8 TeV. Measurements of the total cross section for $t\bar{t}$-production from ATLAS and CMS reach by now an accuracy of typically better than $O(10\%)$, with the systematic and luminosity uncertainties already dominating over the small statistical uncertainty, see, e.g., [1–3]. First results of differential distributions for $t\bar{t}$-production from the LHC are appearing as well [4, 5]. Thus, given the present experimental accuracy hadro-production of $t\bar{t}$-pairs is currently being established as a Standard Model (SM) benchmark process.

This has motivated tremendous activity on the theory side to match the experimental precision by computing higher order corrections in Quantum Chromodynamics (QCD) and we briefly recapitulate the status for inclusive $t\bar{t}$-pair production, i.e., no additional jets or other tagged final states. Predictions for the total cross section are complete to next-to-next-to-leading order (NNLO) [6–9] while differential distributions are known to next-to-leading order (NLO) [10, 11], including top-quark decay [12, 13], though. Additional corrections beyond NLO based on threshold logarithms have been obtained for distributions in the top-quark's transverse momentum and rapidity, p_T^t and y^t, as well as in the invariant mass $m^{t\bar{t}}$ of the top-quark pair [14, 15].

Comparison of these theory predictions to experimental data can be used to determine non-perturbative parameters such as the strong coupling constant, the parton luminosity and the top-quark mass and to study their correlations. Of these parameters, the top-quark mass is certainly the most interesting one with prominent implications for the electro-weak vacuum of the SM, see, e.g., [16, 17]. It is a particularly attractive feature of cross sections measurements that they offer the opportunity for an unambiguous and theoretically well-defined determination of the top-quark mass in a particular renormalization scheme [18, 19].

The conventional scheme choice for the quark mass renormalization is the pole mass, which has its short-comings [20, 21], though, since it is based on the idea of quarks appearing as asymptotic states. It exhibits poor convergence of the perturbative series and due to the renormalon ambiguity it carries an intrinsic uncertainty of the order of $\Lambda_{\rm QCD}$. As an alternative, one can consider top-quark hadro-production with a running mass, which has the advantages of improved convergence and scale stability of the perturbative expansion. For $t\bar{t}$ hadro-production, these features have been demonstrated for the total cross section [18].

In the present letter, we study the dependence of single differential distributions in p_T^t, y^t and $m^{t\bar{t}}$ on the definition of the mass parameter. Specifically, we will compare the conventional pole mass $m_t^{\rm pole}$ with the scale dependent $\overline{\rm MS}$ mass by means of the well-known relation in perturbation theory,

$$m_t^{\rm pole} = m(\mu_r)\left(1+\frac{\alpha_s}{\pi}d_1+\left(\frac{\alpha_s}{\pi}\right)^2 d_2+\ldots\right), \tag{1}$$

for the scheme change from $m_t^{\rm pole}$ to the running $\overline{\rm MS}$ mass $m(\mu_r)$ taken at the renormalization scale μ_r. To NNLO the coefficients d_1 and d_2 are given by [22] (see also Refs. [23, 24])

$$d_1 = \frac{4}{3}+\ell \tag{2}$$

$$d_2 = \frac{307}{32}+\frac{\pi^2}{3}+\frac{\pi^2}{9}\ln(2)-\frac{1}{6}\zeta_3+\frac{509}{72}\ell+\frac{47}{24}\ell^2 - n_f\left(\frac{71}{144}+\frac{\pi^2}{18}+\frac{13}{36}\ell+\frac{1}{12}\ell^2\right), \tag{3}$$

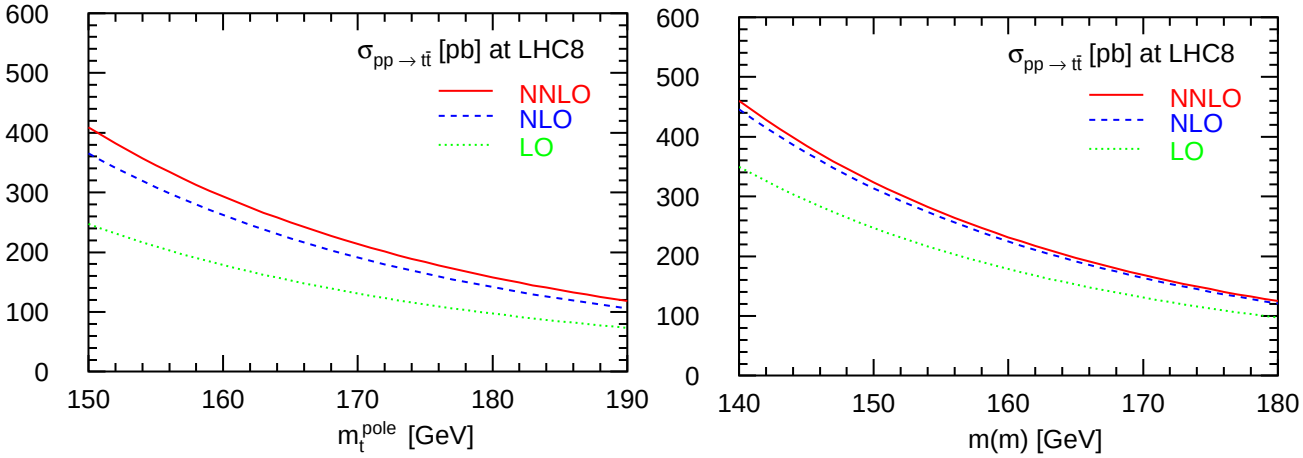

Figure 1: The LO, NLO and NNLO QCD predictions for the total cross section at LHC ($\sqrt{S} = 8$ TeV) as a function of the top-quark mass in the on-shell scheme $m_t^{\rm pole}$ at the scale $\mu = m_t^{\rm pole}$ (left) and, respectively, in the $\overline{\rm MS}$ scheme $m(m)$ at the scale $\mu = m(m)$ (right) using the PDF set ABM11 [25] and $\mu = \mu_r = \mu_f$.

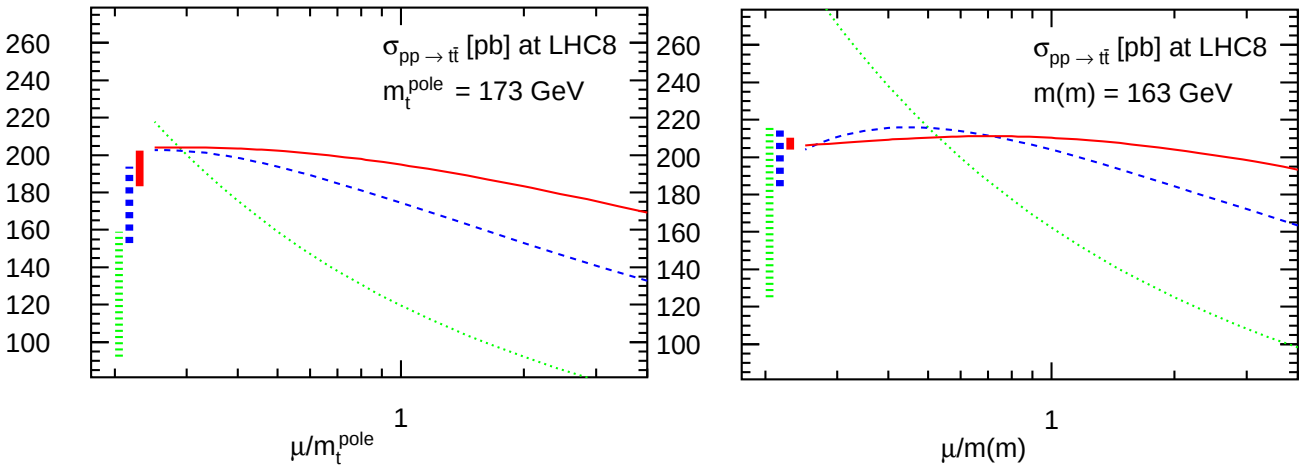

Figure 2: The scale dependence of the LO, NLO and NNLO QCD predictions for the total cross section at LHC ($\sqrt{S} = 8$ TeV) for the top-quark mass $m_t^{\rm pole} = 173$ GeV in the on-shell scheme (left) and for $m(m) = 163$ GeV in the $\overline{\rm MS}$ scheme (right) with the choice $\mu = \mu_r = \mu_f$ using the PDF set ABM11 [25]. The vertical bars indicate the size of the scale variation in the standard range $\mu/m_t^{\rm pole} \in [1/2, 2]$ and $\mu/m(m) \in [1/2, 2]$, respectively.

with $\ell = \ln\left(\frac{\mu_r^2}{m(\mu_r)^2}\right)$ and assuming vanishing masses for all lighter quarks.

Let us briefly illustrate the advantages of the running $\overline{\rm MS}$ mass $m(\mu_r)$ for the total $t\bar{t}$ cross section. The recently completed exact NNLO QCD result [6–9] turned out to be very close, i.e., within $\mathcal{O}(1-2\%)$, to previous approximations based on the combined threshold and high-energy asymptotics [26] and has been presented as a function of the pole mass $m_t^{\rm pole}$. The necessary scheme transformation from $m_t^{\rm pole}$ to $m(\mu_r)$, i.e., the application of eq. (1), has been discussed in [18] and is implemented in the program `Hathor` (version 1.5) [27], a tool for the calculation of

the total $t\bar{t}$ cross section in hadronic collisions.

The much improved apparent convergence of the perturbative expansion with the running mass as well as the scale stability are illustrated in Figs. 1 and 2 where we compare theory predictions for the total $t\bar{t}$ cross section as a function of the pole and the $\overline{\rm MS}$ mass, respectively. Fig. 1 displays the increase in the cross section values from LO to NNLO, where we have taken the parton distribution functions (PDFs) to be order independent. For an on-shell mass $m_t^{\rm pole} = 173$ GeV, for instance, the relative increase is $\sigma_{\rm NLO}/\sigma_{\rm LO} = 1.46$ and $\sigma_{\rm NNLO}/\sigma_{\rm NLO} = 1.12$ at the scale $\mu_r = \mu_f = m_t^{\rm pole}$. This is to be compared with a much reduced increase of only $\sigma_{\rm NLO}/\sigma_{\rm LO} = 1.26$ and $\sigma_{\rm NNLO}/\sigma_{\rm NLO} = 1.03$ for $m(m) = 163$ GeV in the $\overline{\rm MS}$ scheme at the scale $\mu_r = \mu_f = m(m)$. These findings can be understood by noting that the scheme transformation of eq. (1) applied to the total $t\bar{t}$ cross section effectively shifts all parton-level corrections to the threshold region thereby improving the apparent convergence of the perturbation series, see, e.g., [28].

Fig. 2 shows the scale stability for the LHC predictions confirming earlier findings for the Tevatron, cf. [18]. The scale variation for the cross section in the on-shell scheme in the standard range $\mu/m_t^{\rm pole} \in [1/2, 2]$ amounts to $\Delta\sigma_{\rm NNLO} = ^{+3.8\%}_{-6.0\%}$, whereas for the running mass we only find $\Delta\sigma_{\rm NNLO} = ^{+0.1\%}_{-3.0\%}$ for the range $\mu/m(m) \in [1/2, 2]$. Interestingly, for an on-shell mass the point of minimal sensitivity where $\sigma_{\rm LO} \simeq \sigma_{\rm NLO} \simeq \sigma_{\rm NNLO}$ is located at fairly low scales, $\mu \simeq m_t^{\rm pole}/4 \simeq$ 45 GeV, whereas for a running mass it resides at the scale $\mu = \mathcal{O}(m(m))$, i.e., it coincides with the natural hard scale of the process. These results imply, that experimental determinations of the running mass from the measured cross section are feasible with very good accuracy and a small residual theoretical uncertainty. For Tevatron data such analyses have already been performed in the past [17, 29].

For completeness, we include here values for the full NNLO cross sections at the Tevatron ($\sqrt{S} = 1.96$ TeV) and at the LHC for various energies of interest.

	TEV $\sqrt{S} = 1.96$ TeV	LHC $\sqrt{S} = 7$ TeV	LHC $\sqrt{S} = 8$ TeV	LHC $\sqrt{S} = 14$ TeV
ABM11	$6.82\ ^{+0.21\ +0.16}_{-0.29\ -0.16}$	$133.0\ ^{+5.2\ +6.5}_{-8.2\ -6.5}$	$194.9\ ^{+7.4\ +8.8}_{-11.7\ -8.8}$	$821.0\ ^{+27.0\ +25.7}_{-43.7\ -25.7}$
CT10	$7.30\ ^{+0.28\ +0.45}_{-0.39\ -0.33}$	$168.9\ ^{+6.9\ +13.5}_{-10.9\ -10.9}$	$241.6\ ^{+9.5\ +16.9}_{-15.1\ -13.8}$	$939.3\ ^{+32.4\ +37.5}_{-51.7\ -33.3}$

Table 1: The total cross section for top-quark pair-production at NNLO using a pole mass $m_t^{\rm pole} = 173$ GeV and the PDF set ABM11 [25] and CT10 [30] and with the errors shown as $\sigma + \Delta\sigma_{\rm scale} + \Delta\sigma_{\rm PDF}$. The scale uncertainty $\Delta\sigma_{\rm scale}$ is based on maximal and minimal shifts for the choices $\mu = m_t^{\rm pole}/2$ and $\mu = 2m_t^{\rm pole}$ and $\Delta\sigma_{\rm PDF}$ is the 1σ combined PDF+α_s error. All rates are in pb.

	TEV $\sqrt{S} = 1.96$ TeV	LHC $\sqrt{S} = 7$ TeV	LHC $\sqrt{S} = 8$ TeV	LHC $\sqrt{S} = 14$ TeV
ABM11	$7.22\ ^{+0.10\ +0.16}_{-0.10\ -0.16}$	$143.8\ ^{+0.2\ +6.4}_{-4.3\ -6.4}$	$210.4\ ^{+0.1\ +8.6}_{-6.3\ -8.6}$	$880.0\ ^{+0.0\ +24.6}_{-24.0\ -24.6}$
CT10	$7.70\ ^{+0.10\ +0.47}_{-0.15\ -0.35}$	$180.7\ ^{+0.0\ +13.7}_{-5.8\ -11.1}$	$258.0\ ^{+0.0\ +17.2}_{-8.1\ -14.1}$	$997.9\ ^{+0.0\ +38.1}_{-28.3\ -33.9}$

Table 2: Same as Tab. 1 for a running mass $m(m) = 163$ GeV in the $\overline{\rm MS}$ scheme.

Next we discuss the single-differential distributions in the top-quark's transverse momentum p_T^t and rapidity y^t and in the invariant mass $m^{t\bar{t}}$ of the $t\bar{t}$-pair, which are all known to NLO in

QCD [10, 11] in the conventional pole mass scheme. As we are interested in the differential cross sections with the mass in the $\overline{\rm MS}$ scheme, we briefly recall the kinematics of heavy-quark hadroproduction,

$$h_1(P_1) + h_2(P_2) \quad \longrightarrow \quad {\rm Q}(p_1) + X[\overline{\rm Q}](p_X)\,, \tag{4}$$

where h_1 and h_2 are hadrons, $X[\overline{\rm Q}]$ denotes any allowed hadronic final state containing at least the heavy anti-quark, and ${\rm Q}(p_1)$ is the identified heavy-quark with mass m. The hadronic invariants in this reaction are

$$S = (P_1+P_2)^2 \quad , \quad T_1 = (P_2-p_1)^2 - m^2 \quad , \quad U_1 = (P_1-p_1)^2 - m^2\,. \tag{5}$$

The double differential cross section for eq. (5) in terms of the hard parton cross section σ_{ij} and PDFs f_i at the factorization scale μ^2 reads

$$S^2\frac{d^2\sigma(S,T_1,U_1)}{dT_1dU_1} = \int_{x_1^-}^1 \frac{dx_1}{x_1}\int_{x_2^-}^1 \frac{dx_2}{x_2} f_i(x_1,\mu^2)\,f_j(x_2,\mu^2) s^2 \frac{d^2\sigma_{ij}(s,t_1,u_1,\mu^2)}{dt_1du_1}\,, \tag{6}$$

and the partonic invariants are related to their hadronic counterparts through

$$t_1 = x_1T_1\,, \qquad\qquad u_1 = x_2U_1\,, \qquad\qquad s = x_1x_2S\,, \tag{7}$$

with the limits on x_1 and x_2,

$$x_1^- = -\frac{U_1}{S+T_1} \le x_1 \le 1\,, \qquad\qquad x_2^- = \frac{x_1T_1}{x_1S+U_1} \le x_2 \le 1\,. \tag{8}$$

In order to write the differential cross section in terms of p_T^t, y^t and $m^{t\bar{t}}$, we will also need their definitions in terms of the hadronic invariants. For the case of p_T^t and y^t, the relations are

$$y^t = \frac{1}{2}\ln\left(\frac{T_1}{U_1}\right)\,, \qquad\qquad (p_T^t)^2 = \frac{T_1U_1}{S} - m^2\,, \tag{9}$$

whereas for $m^{t\bar{t}}$, pair-invariant mass kinematics is used, in which case the requirements on the integrals are

$$x_1^- = \frac{\left(m^{t\bar{t}}\right)^2}{S} \qquad \text{and} \qquad x_2^- = \frac{\left(m^{t\bar{t}}\right)^2}{x_1S}\,. \tag{10}$$

In these kinematics, the relevant partonic invariants for writing the differential cross section in terms of $m^{t\bar{t}}$ are,

$$t_1 = -\frac{\left(m^{t\bar{t}}\right)^2}{2}\left(1-\beta_t\cos\theta\right)\,, \qquad\qquad u_1 = -\frac{\left(m^{t\bar{t}}\right)^2}{2}\left(1+\beta_t\cos\theta\right)\,, \tag{11}$$

with $\beta_t = \sqrt{1-4m^2/\left(m^{t\bar{t}}\right)^2}$ and θ the scattering angle of the top quark. Full discussions of the kinematics to NLO for one-particle inclusive and pair-invariant mass kinematics are available in [11, 31] respectively.

In order to convert to cross section predictions with the mass in the $\overline{\text{MS}}$ scheme, we start from the on-shell description:

$$\frac{d\sigma(m_t^{\text{pole}})}{dX} = \left(\frac{\alpha_s}{\pi}\right)^2 \frac{d\sigma^{(0)}(m_t^{\text{pole}})}{dX} + \left(\frac{\alpha_s}{\pi}\right)^3 \frac{d\sigma^{(1)}(m_t^{\text{pole}})}{dX} + O(\alpha_s^2), \tag{12}$$

where X denotes any of the variables p_T^t, y^t and so on. If we now replace m_t^{pole} with $m(\mu_r)$ using eq. (1), we can expand in α_s and obtain a description of the differential cross section in the $\overline{\text{MS}}$ scheme.

$$\begin{aligned}\frac{d\sigma(m(\mu_r))}{dX} &= \left(\frac{\alpha_s}{\pi}\right)^2 \frac{d\sigma^{(0)}(m(\mu_r))}{dX} \\ &+ \left(\frac{\alpha_s}{\pi}\right)^3 \left\{ \frac{d\sigma^{(1)}(m(\mu_r))}{dX} + d_1 m(\mu_r) \frac{d}{dm_t} \left(\frac{d\sigma^{(0)}(m_t)}{dX} \right) \Big|_{m_t = m(\mu_r)} \right\} + O(\alpha_s^2).\end{aligned} \tag{13}$$

The only extra part required is the mass derivative of the Born contribution. This has been computed semi-analytically for the p_T^t, y^t, and $m^{t\bar{t}}$ distributions. To see why we also need some numerical derivatives in this calculation, consider eq. (6) for the Born contribution to the double differential cross section as a starting point:

$$\int_{x_1^-}^1 \frac{dx_1}{x_1} \int_{x_2^-}^1 \frac{dx_2}{x_2} f_i(x_1,\mu^2) f_j(x_2,\mu^2) s^2 \frac{d^2\sigma_{ij}^{(0)}}{dt_1 du_1} \delta(s+t_1+u_1), \tag{14}$$

where the delta function imposes Born kinematics and can be used to carry out the integral over x_2 through its relation to s, t_1 and u_1. Re-writing the cross section in terms of p_T^t and y^t provides us with the form of the integrand that will need to be evaluated,

$$\int_{x_1^-}^1 dx_1 \mathcal{L}(x_1,x_2,\mu^2) \frac{x_1 x_2 S}{x_1 S + U_1} \left. \frac{d^2\sigma(s,t_1,u_1)}{dy^t dp_T^{t2}} \right|_{x_2 = -\frac{x_1 T_1}{x_1 S + U_1}}, \tag{15}$$

where $\mathcal{L}(x_1,x_2,\mu^2) = f_1(x_1,\mu^2) f_2(x_2,\mu^2)/x_1 x_2$ is the differential parton luminosity.

The most important aspect to note is that both x_2 and x_1^- depend on the top-quark mass through their relations to the Mandelstam variables. This means that the mass derivative of the PDFs needs to be done numerically using

$$\begin{aligned}\frac{d}{dm}\mathcal{L}(x_1,x_2,\mu^2) &= \frac{dx_1}{dm} \frac{\mathcal{L}(x_1+\delta,x_2,\mu^2) - \mathcal{L}(x_1-\delta,x_2,\mu^2)}{2\delta} \\ &+ \frac{dx_2}{dm} \frac{\mathcal{L}(x_1,x_2+\delta,\mu^2) - \mathcal{L}(x_1,x_2-\delta,\mu^2)}{2\delta}.\end{aligned} \tag{16}$$

This form of the derivative is found to converge well. Aside from this, all other derivatives are known analytically. When compared with a fully numerical calculation of the derivative term, it is found that the two methods agree to less than 1%. In the case of $m^{t\bar{t}}$, the integration limits and variables do not depend on the top-quark mass (m) so all derivatives are computed analytically.

Using the relations presented here, we have computed the differential cross sections for $t\bar{t}$-production in terms of p_T^t, y^t and $m^{t\bar{t}}$. We have used the program `MCFM` [32] for the NLO corrections [13, 33] in the conventional pole mass m_t^{pole} scheme and a custom routine for the Born and

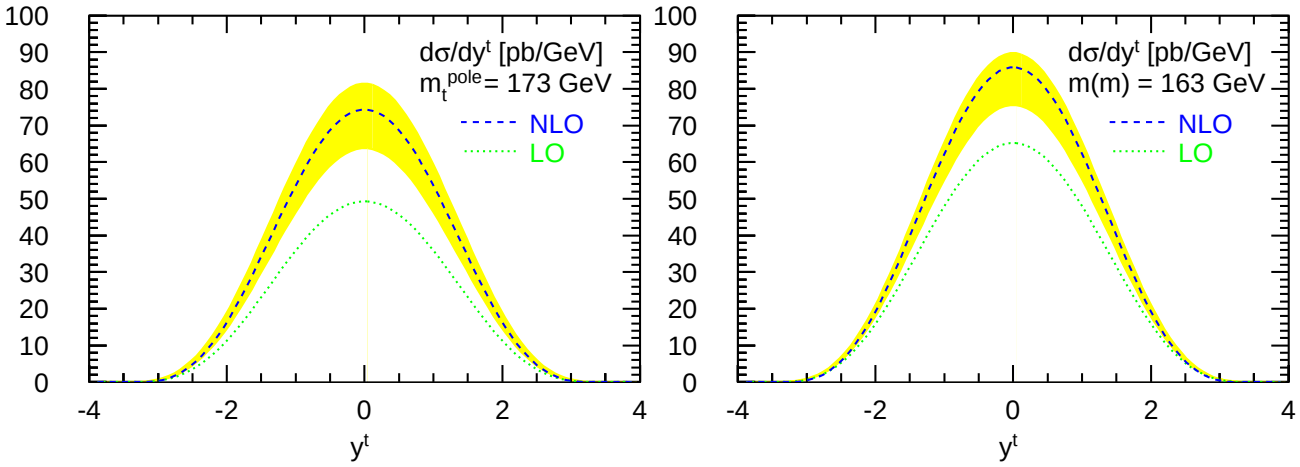

Figure 3: The differential cross section with respect to the rapidity y^t of the top quark in the pole (left) and the $\overline{\text{MS}}$ (right) mass scheme at the LHC with $\sqrt{S} = 8$ TeV. The dotted (green) curves are the LO contributions while the dashed (blue) curves include NLO corrections and are obtained using the PDF set CT10 [30]. The scale dependence in the range μ/m_t^{pole} or $\mu/m(m) \in [1/2, 2]$ is shown as a band around the NLO curve.

mass derivative terms. The calculations were carried out using the ABM11 [25] and CT10 [30] PDFs at NLO. As a check, each curve was integrated to obtain a result for the full cross section. In all cases, the value agreed within less than 1% of the cross section computed using `Hathor`. As well, the mass derivatives were checked by computing the differential cross sections at values of the top mass ranging between 150 GeV and 180 GeV. A curve was fit to each point in the relevant spectrum to obtain the derivative at the given $\overline{\text{MS}}$ mass. Again, these values agreed within less than 1% of the (semi-)analytic derivatives used.

In Fig. 3 the rapidity distributions are shown for the $\overline{\text{MS}}$ and pole mass schemes. It is clear from these that at NLO, the convergence of the perturbative series as well as the scale dependence improves. In the pole-mass scheme, a relative increase for the cross section ratios $\sigma_{\text{NLO}}/\sigma_{\text{LO}} = 1.50$ is seen, while in the $\overline{\text{MS}}$ scheme we have $\sigma_{\text{NLO}}/\sigma_{\text{LO}} = 1.31$ at $y^t = 0$. The scale variation in the on-shell scheme is $\Delta\sigma_{\text{NLO}} = {}^{+9.5\%}_{-14\%}$ while in the $\overline{\text{MS}}$ scheme, we have $\Delta\sigma_{\text{NLO}} = {}^{+4.5\%}_{-12\%}$ again at $y^t = 0$.

Fig. 4 shows the transverse momentum distributions. Again we see an improvement when moving from the pole mass scheme to the $\overline{\text{MS}}$ scheme. In this case the improvement in the NLO contribution is a bit better with $\sigma_{\text{NLO}}/\sigma_{\text{LO}} = 1.50$ for the pole mass scheme and $\sigma_{\text{NLO}}/\sigma_{\text{LO}} = 1.25$ in the $\overline{\text{MS}}$ scheme. The scale variation goes from $\Delta\sigma_{\text{NLO}} = {}^{+13\%}_{-13\%}$ in the pole mass scheme to $\Delta\sigma_{\text{NLO}} = {}^{+6.4\%}_{-9.6\%}$ in the $\overline{\text{MS}}$ scheme. The above values are taken near the maximum of the curve at $p_T^t = 75$ GeV.

Finally, in Fig. 5 we show the invariant mass distributions. The increase at NLO here is $\sigma_{\text{NLO}}/\sigma_{\text{LO}} = 1.54$ with scale variation $\Delta\sigma_{\text{NLO}} = {}^{+13\%}_{-13\%}$ in the pole mass scheme and $\sigma_{\text{NLO}}/\sigma_{\text{LO}} = 1.30$ with scale variation $\Delta\sigma_{\text{NLO}} = {}^{+8.2\%}_{-9.6\%}$ in the $\overline{\text{MS}}$ scheme. These values are taken at an invariant mass of $m^{t\bar{t}} = 137$ GeV.

In addition to these improvements, moving from the pole mass to the $\overline{\text{MS}}$ scheme changes the overall shape of the distributions so that the peak positions generally become more pronounced. This is a consequence of the radiative corrections being shifted to the threshold region as mentioned

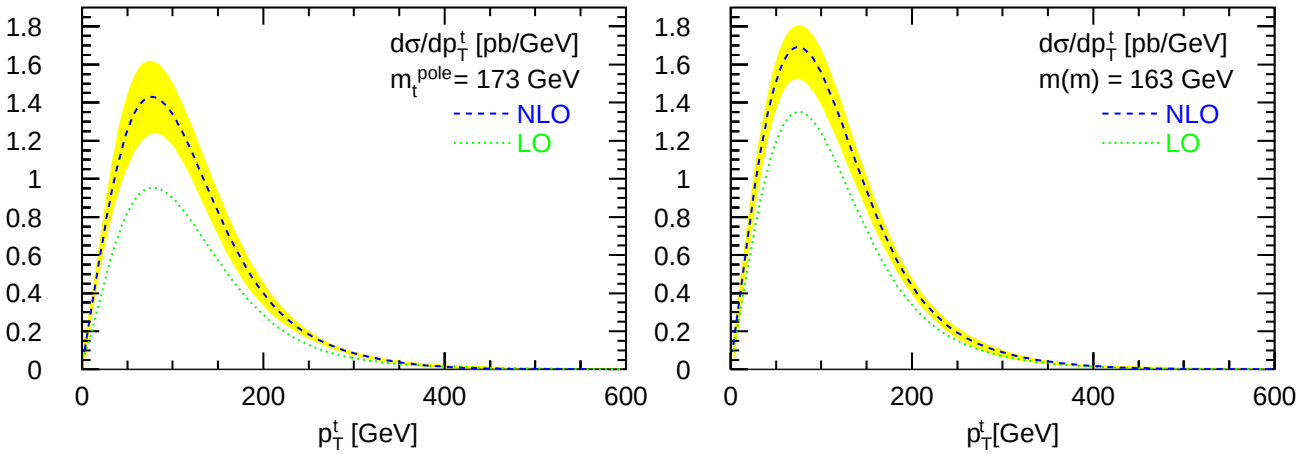

Figure 4: Same as Fig. 3 for the differential cross section with respect to the transverse momentum p_T^t of the top quark.

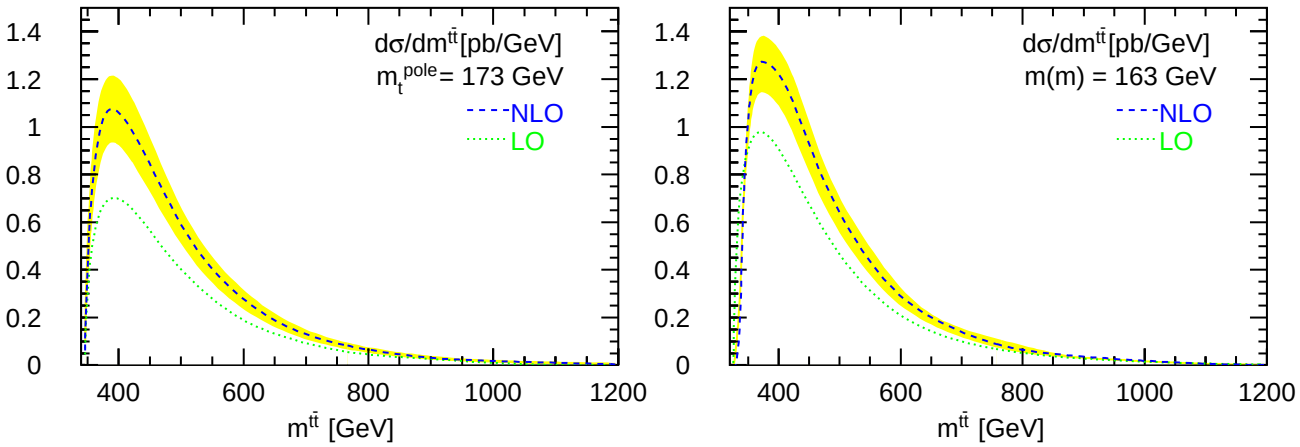

Figure 5: Same as Fig. 3 for the differential cross section with respect to the invariant mass $m^{t\bar{t}}$ of the top quark pair.

earlier. However, the peak positions in both the p_T^t and $m^{t\bar{t}}$ distributions are stable against radiative corrections. At most they are seen to shift by 1%, which is unlike the case for $t\bar{t}$-production from e^+e^- collisions where the position of the $t\bar{t}$-threshold peak shifts significantly upon adding NLO and NNLO perturbative corrections to the total cross section expressed in terms of the pole mass [34].

Another salient feature not shown in Fig. 5 above occurs in the $\overline{\text{MS}}$ differential cross section with respect to the invariant mass of the $t\bar{t}$ pair. Very close to the threshold of $t\bar{t}$ production the contribution reponsible for the change in the mass renormalization scheme, i.e., the derivative term in eq. (13), becomes large. This is due to the presence of a $1/\beta_t$ which diverges as $m^{t\bar{t}} \to m$, cf. eq. (11). These large corrections have the effect of causing the invariant mass spectrum to dip below zero for values of $m^{t\bar{t}} \gtrsim 2m_t$. In the full spectrum, however, this is counterbalanced by the positive contribution resulting in a cross section integrated over $m^{t\bar{t}}$ that agrees within less than 1% with the value calculated in `Hathor`.

Obviously, this behavior is an indication of the breakdown of fixed-order perturbation theory.

First of all, bound-state effects in $t\bar{t}$ production at hadron colliders arise in the kinematic region $m^{t\bar{t}} \gtrsim 2m_t$, i.e., when the velocity β of the top quarks is small, $\beta \ll 1$. In this region, the conventional perturbative expansion in α_s breaks down, owing to singular terms $\sim (\alpha_s/\beta)^n$ in the n-loop amplitude, which require the all-order resummation of the Coulomb corrections [35, 36]. This resummation for $t\bar{t}$ dynamics close to threshold is carried out in a non-relativistic effective theory by means of a Schrödinger equation for which the pole mass definition seems to be the natural choice and which implies a certain power counting, so that all terms of order $m_t\beta^2 \sim m_t\alpha_s^2$ are formally of equal size.

If the contribution for the change in the mass renormalization scheme $\delta m^{\rm sd}$ from the pole mass to a so-called short-distance mass $m_t^{\rm sd}$ such as the $\overline{\rm MS}$ mass $m(\mu_r)$ is parametrically larger than $m_t\alpha_s^2$ that is $\delta m^{\rm sd} \equiv m_t^{\rm pole} - m^{\rm sd} \sim m_t^{\rm sd}\alpha_s$, then $\delta m^{\rm sd}$ becomes the dominant term in the kinematic region $m^{t\bar{t}} \gtrsim 2m_t$. Such situation is realized for $\delta m^{\rm sd} \sim m_t\alpha_s$, cf. eq. (13), and excludes the $\overline{\rm MS}$ mass from being a useful mass near threshold. Of course, all these findings on the scheme choice for the mass definition close to the threshold are long known from studies for $t\bar{t}$ production in e^+e^- collisions [34]. Various solutions have been proposed, e.g., the alternative use of a so-called $1S$ mass [37] defined through the perturbative contribution to the mass of a hypothetical $n = 1$, ${}^3S_1$ toponium bound state, cf. [38] for an application to $t\bar{t}$ hadro-production or the use of a "potential-subtracted" (PS) mass [39], recently considered in [40] in the context of finite-width effects in unstable-particle production at hadron colliders. In any case, since the conventional perturbative expansion of the cross section breaks down for $m^{t\bar{t}} \gtrsim 2m_t$ we do not display this particular kinematic region in Fig. 5. Moreover, with the currently given experimental resultion for the $m^{t\bar{t}}$-bins, cf. [4], it will be difficult to access this region at the LHC at all.

For completeness we also provide a table of values for the cross section at LHC with $\sqrt{S} =$ 8 TeV at binned values of y^t, p_T^t and $m^{t\bar{t}}$ with binning approximately equal to that of [4]. Comparing the data generated using ABM11 as compared to CT10, we see that there is an overall shift downward consistent with that observed for the total cross section, cf. Tabs. 1 and 2. The improvement of the apparent perturbative convergence and the scale stability when moving from the pole mass scheme to the $\overline{\rm MS}$ scheme is consistent for both PDF sets.

	$m_t^{\rm pole}$		$m(m)$	
$\frac{d\sigma}{dy^t}$	LO	NLO	LO	NLO
$y^t = 0.2$	48.70	73.43	64.46	84.83
$y^t = 0.6$	44.12	66.34	58.57	76.74
$y^t = 1.0$	35.90	53.70	48.00	62.29
$y^t = 1.4$	25.77	38.19	34.87	44.51
$y^t = 2.0$	11.37	16.39	15.93	19.34

Table 3: Values for the y^t differential cross section for top-quark pair-production at LO and NLO for various y^t using the PDF set CT10 [30] with $\sqrt{S} = 8$TeV. All rates are in pb.

In summary, we have shown how treating the differential cross sections for $t\bar{t}$ production in the $\overline{\rm MS}$ scheme for the top-quark mass has benefits as compared to the pole mass scheme. The

	$m_t^{\rm pole}$		$m(m)$	
$\frac{d\sigma}{dp_T^t}$	LO	NLO	LO	NLO
$y^t = 0.2$	44.39	65.82	59.51	76.33
$y^t = 0.6$	39.55	58.57	53.18	68.00
$y^t = 1.0$	31.07	45.89	42.06	53.44
$y^t = 1.4$	21.04	30.91	28.83	36.18
$y^t = 2.0$	8.018	11.55	11.40	13.72

Table 4: The same as table 3 but using the PDF set ABM11 [25] .

	$m_t^{\rm pole}$		$m(m)$	
$\frac{d\sigma}{dp_T^t}$	LO	NLO	LO	NLO
$p_T^t = 30\texttt{GeV}$	0.5513	0.8681	0.8214	1.058
$p_T^t = 90\texttt{GeV}$	0.9364	1.399	1.308	1.637
$p_T^t = 130\texttt{GeV}$	0.7130	1.045	0.9419	1.196
$p_T^t = 170\texttt{GeV}$	0.4422	0.6288	0.5455	0.7057
$p_T^t = 230\texttt{GeV}$	0.1777	0.2496	0.2070	0.2675
$p_T^t = 290\texttt{GeV}$	0.06806	0.09941	0.08152	0.1035
$p_T^t = 360\texttt{GeV}$	0.02533	0.03105	0.02756	0.03537

Table 5: Values for the p_T^t differential cross section for top-quark pair-production at LO and NLO for various p_T^t using the PDF set CT10 [30]. All rates are in pb/GeV.

	$m_t^{\rm pole}$		$m(m)$	
$\frac{d\sigma}{dp_T^t}$	LO	NLO	LO	NLO
$p_T^t = 30\texttt{GeV}$	0.4874	0.7568	0.7467	0.9220
$p_T^t = 90\texttt{GeV}$	0.8141	1.206	1.148	1.429
$p_T^t = 130\texttt{GeV}$	0.6076	0.8862	0.8053	1.006
$p_T^t = 170\texttt{GeV}$	0.3658	0.5262	0.4429	0.5843
$p_T^t = 230\texttt{GeV}$	0.1425	0.1954	0.1750	0.2175
$p_T^t = 290\texttt{GeV}$	0.05567	0.06975	0.06227	0.07316
$p_T^t = 360\texttt{GeV}$	0.02008	0.02415	0.01266	0.01818

Table 6: The same as table 5 but using the PDF set ABM11 [25] .

perturbative series shows the same improvement in convergence and scale dependence as has been observed for the total cross section. As a consequence the NLO contributions with a $\overline{\rm MS}$ mass are expected to provide already very precise cross section predictions. An extension to NNLO

	$m_t^{\rm pole}$		$m(m)$	
$\frac{d\sigma}{dm^{t\bar{t}}}$	LO	NLO	LO	NLO
$m^{t\bar{t}} = 350\texttt{GeV}$	0.2985	0.4278	0.9046	1.0295
$m^{t\bar{t}} = 450\texttt{GeV}$	0.5648	0.8441	0.6755	0.9270
$m^{t\bar{t}} = 500\texttt{GeV}$	0.4022	0.5914	0.4656	0.6403
$m^{t\bar{t}} = 600\texttt{GeV}$	0.1898	0.2782	0.2102	0.2917
$m^{t\bar{t}} = 700\texttt{GeV}$	0.09342	0.1301	0.09977	0.1404
$m^{t\bar{t}} = 950\texttt{GeV}$	0.01796	0.02343	0.02067	0.02740

Table 7: Values for the $m^{t\bar{t}}$ differential cross section for top-quark pair-production at LO and NLO for various $m^{t\bar{t}}$ using the PDF set CT10 [30]. All rates are in pb/GeV.

	$m_t^{\rm pole}$		$m(m)$	
$\frac{d\sigma}{dm^{t\bar{t}}}$	LO	NLO	LO	NLO
$m^{t\bar{t}} = 350\texttt{GeV}$	0.3036	0.4546	0.8420	0.9508
$m^{t\bar{t}} = 450\texttt{GeV}$	0.4967	0.7381	0.5914	0.8103
$m^{t\bar{t}} = 500\texttt{GeV}$	0.3481	0.5118	0.3964	0.54488
$m^{t\bar{t}} = 600\texttt{GeV}$	0.1554	0.2212	0.1704	0.2357
$m^{t\bar{t}} = 700\texttt{GeV}$	0.0729	0.09674	0.07706	0.1061
$m^{t\bar{t}} = 950\texttt{GeV}$	0.01326	0.01839	0.01407	0.01611

Table 8: The same as table 7 but using the PDF set ABM11 [25] .

accuracy would provide results with a still smaller theoretical uncertainty from the scale variation. Yet, the predictions at the nominal scale, i.e., $\mu_r = m(m)$, are expected to remain largely unchanged.

As future prospects we note that the refinement of the present phenomenological analysis to NNLO accuracy is certainly feasible once the complete NNLO QCD corrections for differential $t\bar{t}$ production are available. As a first step in this direction, one may consider approximate NNLO corrections based, e.g., on the dominant threshold logarithms. Other obvious improvements are extension to double-differential distributions and other exclusive observables, even including top-quark decay.

Acknowledgments

This work is partially supported by the Deutsche Forschungsgemeinschaft in Sonderforschungsbereich/Transregio 9 and by the European Commission through contract PITN-GA-2010-264564 (*LHCPhenoNet*).

References

[1] CMS Collaboration, (2012), CMS-PAS-TOP-12-003.

[2] ATLAS Collaboration, (2012), ATLAS-CONF-2012-149, ATLAS-COM-CONF-2012-170.

[3] CMS Collaboration, (2012), CMS-PAS-TOP-12-006.

[4] CMS Collaboration, S. Chatrchyan *et al.*, Eur.Phys.J. **C73**, 2339 (2013), arXiv:1211.2220.

[5] ATLAS Collaboration, G. Aad *et al.*, Eur.Phys.J. **C73**, 2261 (2013), arXiv:1207.5644.

[6] P. Bärnreuther, M. Czakon, and A. Mitov, Phys.Rev.Lett. **109**, 132001 (2012), arXiv:1204.5201.

[7] M. Czakon and A. Mitov, JHEP **1212**, 054 (2012), arXiv:1207.0236.

[8] M. Czakon and A. Mitov, JHEP **1301**, 080 (2013), arXiv:1210.6832.

[9] M. Czakon, P. Fiedler, and A. Mitov, (2013), arXiv:1303.6254.

[10] W. Beenakker, H. Kuijf, W. van Neerven, and J. Smith, Phys.Rev. **D40**, 54 (1989).

[11] M. L. Mangano, P. Nason, and G. Ridolfi, Nucl.Phys. **B373**, 295 (1992).

[12] K. Melnikov and M. Schulze, JHEP **0908**, 049 (2009), arXiv:arXiv:0907.3090.

[13] J. M. Campbell and R. K. Ellis, (2012), arXiv:1204.1513.

[14] N. Kidonakis, Phys.Rev. **D82**, 114030 (2010), arXiv:1009.4935.

[15] V. Ahrens *et al.*, Phys.Lett. **B687**, 331 (2010), arXiv:0912.3375.

[16] F. Bezrukov, M. Y. Kalmykov, B. A. Kniehl, and M. Shaposhnikov, JHEP **1210**, 140 (2012), arXiv:1205.2893.

[17] S. Alekhin, A. Djouadi, and S. Moch, Phys.Lett. **B716**, 214 (2012), arXiv:1207.0980.

[18] U. Langenfeld, S. Moch, and P. Uwer, Phys.Rev. **D80**, 054009 (2009), arXiv:0906.5273.

[19] S. Alioli *et al.*, (2013), arXiv:1303.6415.

[20] I. I. Bigi, M. A. Shifman, N. Uraltsev, and A. Vainshtein, Phys.Rev. **D50**, 2234 (1994), arXiv:hep-ph/9402360.

[21] M. Beneke and V. M. Braun, Nucl.Phys. **B426**, 301 (1994), arXiv:hep-ph/9402364.

[22] N. Gray, D. J. Broadhurst, W. Grafe, and K. Schilcher, Z.Phys. **C48**, 673 (1990).

[23] K. Chetyrkin and M. Steinhauser, Nucl.Phys. **B573**, 617 (2000), arXiv:hep-ph/9911434.

[24] K. Melnikov and T. v. Ritbergen, Phys.Lett. **B482**, 99 (2000), arXiv:hep-ph/9912391.

[25] S. Alekhin, J. Blümlein, and S. Moch, Phys.Rev. **D86**, 054009 (2012), arXiv:1202.2281.

[26] S. Moch, P. Uwer, and A. Vogt, Phys.Lett. **B714**, 48 (2012), arXiv:1203.6282.

[27] M. Aliev *et al.*, Comput.Phys.Commun. **182**, 1034 (2011), arXiv:1007.1327.

[28] S. Moch, U. Langenfeld, and P. Uwer, PoS **RADCOR2009**, 030 (2010), arXiv:1001.3987.

[29] D0 Collaboration, V. M. Abazov *et al.*, Phys.Lett. **B703**, 422 (2011), arXiv:1104.2887.

[30] J. Gao *et al.*, (2013), arXiv:1302.6246.

[31] W. Beenakker *et al.*, Nucl.Phys. **B351**, 507 (1991).

[32] J. M. Campbell, R. Ellis and C. Williams, *MCFM webpage http://mcfm.fnal.gov*.

[33] J. M. Campbell and R. Ellis, Nucl.Phys.Proc.Suppl. **205-206**, 10 (2010), arXiv:1007.3492.

[34] A. Hoang *et al.*, Eur.Phys.J.direct **C2**, 1 (2000), arXiv:hep-ph/0001286.

[35] K. Hagiwara, Y. Sumino, and H. Yokoya, Phys.Lett. **B666**, 71 (2008), arXiv:0804.1014.

[36] Y. Kiyo *et al.*, Eur.Phys.J. **C60**, 375 (2009), arXiv:0812.0919.

[37] A. Hoang and T. Teubner, Phys.Rev. **D60**, 114027 (1999), arXiv:hep-ph/9904468.

[38] V. Ahrens *et al.*, Phys.Lett. **B703**, 135 (2011), arXiv:1105.5824.

[39] M. Beneke, Phys.Lett. **B434**, 115 (1998), arXiv:hep-ph/9804241.

[40] P. Falgari, A. Papanastasiou, and A. Signer, (2013), arXiv:1303.5299.